

An accessible method of embedding fibre optic sensors on lithium-ion battery surface for in-situ thermal monitoring

Keith M. Alcock^{a,*}, Markus Grammel^a, Álvaro González-Vila^{b,c}, Leonardo Binetti^a, Keng Goh^a, Lourdes S.M. Alwis^a

^a Edinburgh Napier University, UK

^b University of Mons, Belgium

^c IKERLAN Technology Research Centre, Basque Research and Technology Alliance (BRTA), Spain



ARTICLE INFO

Article history:

Received 6 April 2021

Received in revised form 10 August 2021

Accepted 26 August 2021

Available online 1 September 2021

Keywords:

Fibre bragg gratings (FBG)

Fibre optic sensor (FOS)

Lithium-ion battery (LIB)

Thermal monitoring

Constant power (CW)

Guide tube

Electric vehicle (EV)

K-type thermocouples

Temperature measurement

ABSTRACT

Presented is a proof of concept to evaluate the suitability of a mounting technique for fibre optic sensors (FOSs) to measure Lithium-ion Battery (LIB) temperature. Two mounting techniques for the optical fibre, i.e. containing multiple Fibre Bragg Gratings (FBGs), placed on the LIB are considered. The FOS results are compared with K-type thermocouples, which are also mounted on the LIB. The first mounting technique attaches the FBGs on to the battery surface using a binding agent, while for the second technique, a "guide-tube" is used for alleviating longitudinal strain in the FOS induced by LIB expansion without the complexity of metal or glass tubes typically used for signal decoupling. The first mounting technique is calibrated over a 40 °C temperature variation to derive the sensitivity factor for each FBG; the other technique uses the free fibre sensitivity obtained by the manufacturer. The LIB is subject to 10 Watts constant power (CW) discharge, inducing 14 °C surface temperature increase. The guide-tube technique proposed in this study improves measurement accuracy from ± 4.25 °C to + 2.06 °C when both mounting techniques are directly compared to the thermocouples. The proposed mounting technique is found to be a feasible method for cell-level temperature monitoring applications.

© 2021 Elsevier B.V. All rights reserved.

1. Introduction

GLOBALLY, fossil fuel-based transportation accounts for 14% of human-generated greenhouse gas emissions, resulting in a shift away from carbon-intensive transportation modes [1]. Countries such as France and the UK are to end sales of internal combustion-engine cars in favour of electric vehicles (EV) by 2040, whereas India plans to achieve this by 2030 [2]. In 2017 electric vehicle sales grew from 740,000 the previous year to 1.1 million, a 51% increase, reaching a market share of 1.7%. It is forecast there will be nearly 400 models of EVs and 25 million sales by 2025 [3]. Lithium-Ion Battery (LIB) technology, typically used in EVs, is prevalent in modern-day society as mobile phones, laptops and a plethora of other gadgets rely on LIBs on a day to day basis. The LIB is expected to play an ever-increasing role in more diverse ways with the advancement in

battery technology. One example of this is the aviation industry; manufacturers are deviating towards more electric aircraft (MEA), replacing the conventional systems, typically non-propulsion systems with electrical-based systems. As hydraulic and pneumatic emergency systems migrate to electrical equivalents, the onboard power demand increases, thus, MEA use state of the art LIB technology as these have higher energy density and lower weight [4].

Transport modes such as electric and hybrid buses, EVs, and MEA require medium-to-large scale LIB packs; thus, the safe operation of the LIB is pertinent to the successful deployment of large-scale applications. One main obstacle to this is the multitude of safety concerns when utilising LIBs [5–7]. The environmental conditions and specific usage case in which a LIB is operating can have a role in performance issues[3,8]; therefore the temperature, in particular, is considered a critical safety concern [5,7,9–13]. Accurate temperature measurements can diagnose or prevent LIB failure; unfortunately, to date, there has been a multitude of accidents concerning LIB failure. In 2013 a Boeing 787 Dreamliner developed an abnormal temperature change and pressure build up in a battery cell within its battery pack resulting in smoke and flames in the aircraft [11]. The Mars global surveyor was the victim of LIB failure in 2006; the exposure of

* Corresponding author.

E-mail addresses: k.alcock@napier.ac.uk (K.M. Alcock), 40446285@live.napier.ac.uk (M. Grammel), alvaro.gonzalezvila@umons.ac.be, alvaro.gonzalez@ikerlan.es (Á. González-Vila), l.binetti@napier.ac.uk (L. Binetti), k.goh@napier.ac.uk (K. Goh), l.alwis@napier.ac.uk (L.S.M. Alwis).

the battery pack to high-temperature from sunlight resulted in premature capacity degradation [11]. Studies have shown that when operating a LIB at lower temperatures, energy consumption is significantly reduced [7,14,15]. LIBs require a specific temperature window to work at peak efficiency, which is typically between 20 °C and 40 °C [15]. Temperatures below this range cause a slow reaction rate within the cell, resulting in less current delivery and, thus, reduced performance as well as accelerated ageing effects within the cell, impacting usable life [15], therefore, temperature measurement is an appropriate tool for predicting temperature-induced degradation mechanisms [16,17].

Thermocouples are the most widely used technique for temperature monitoring as they are typically low-cost and have small dimensions [18]. However, in comparison to thermocouples, fibre optic sensors (FOSs) have several advantages, such as electrical passivity and the ability to withstand harsh environments at elevated temperatures [19]. FOSs are typically lightweight, with a smaller physical dimension compared to thermocouples and enable a wider bandwidth of data, which is useful to sensor systems involving the interrogation of a collection of sensing elements or a sensor grid [9]. Applications, i.e. where many measuring points are needed to achieve comprehensive monitoring, can take advantage of the multiplexing capabilities of FOS systems as they can offer multiple monitoring points on a single fibre resulting in minimal wiring requirements with high measuring point densities [20]. In a typical large-scale LIB pack of hundreds or thousands of individual cells, the battery management system (BMS) monitors the temperature of sub-grouped cells, often referred to as modules. LIB failure can occur due to the lack of individual cell monitoring, which is avoidable if a broader range of information about individual cell temperature is available to the BMS [11].

The FOS scheme with multiple fibre Bragg gratings (FBGs) is a promising alternative to obtain battery temperature due to its ability to customise the location of the sensors. Applying multiple photo-inscribed Bragg gratings on one fibre means that individual cell monitoring is an ever-increasing possibility as one optical fibre strand containing multiple sensors could be used to monitor a multitude of cells simultaneously. Pouch cells, a common LIB type, are the subject of investigations using FOSs with FBGs [9,10,21,22]. To date, research on utilising FOSs on cylindrical type LIBs is limited.

Notably, M. Nascimento et al. [23] utilise a Sanyo LITUR18650SAN cell to investigate the real-time monitoring of external temperature and strain variations using FBG sensors under charge and different discharge C-rates. During the discharge process, the study finds strain variations said to be induced by pressure increase within the LIB [23]. Fleming et al. and McTurk et al. take advantage of FOSs to reliably obtain core temperature data from a cylindrical LIB cell [17,24]. Using a single-mode SMF-28, 9/125 mm fibre with four 5 mm FBGs evenly spaced, Fleming et al. were able to record "unprecedented cell data" from the LIB core [17]. McTurk et al. using a silica fibre with a single FBG for LIB Core temperature measurement highlights the linear relationship between the FBG Bragg wavelength, temperature or mechanical strain, where the strain relief is obtained with an aluminium tube [24]. The Bragg reflected wavelength is sensitive to applied strain or temperature changes; this poses a requirement for a method to determine or alleviate strain or temperature, in the form of mechanical relief or by subtracting the difference in wavelength shift measured by a nearby FBG sensor which is isolated from the disturbance in question [24,25].

The work presented herewith investigates an FBG sensor array placed on a Panasonic NCR18650B cylindrical LIB, with a particular focus on the sensor mounting technique. The Panasonic cell model is used as it is widely available commercially, and its form factor and electrical specifications are similar to the LIB Panasonic supplies to Tesla for the Model S EV [26]. The process carried out in this investigation is similar to other studies on the pouch and coin cell

types [9,10] in which a FOS with five FBG sensors is glued to the battery and placed in a thermal chamber. These studies use varying sensor-mounting methods and sensor arrangements. For example, in [10], a pouch cell is monitored with 3 FBGs and three thermocouples with three glue spots evenly distributed along the length; and in [9], coin cells with FBG sensors were placed at the positive and negative terminals, with thermocouples used for comparability.

The work herein differs from the examples discussed above, in terms of isolating the temperature reading from the strain induced on the fibre using a "guide-tube" mounting method. The FBG is able to measure temperature and strain simultaneously; thus, the two measurements must be decoupled, typically carried out using a metal or glass cylinder as strain relief [17,24]. The adhesion of the sensors onto the battery surface is an essential aspect as the battery expansion, and contraction, i.e. resulting from variations in the internal pressure, could influence the temperature measurement, in that the strain-induced variation would read as a temperature fluctuation [23,25]. The two mounting methods explored in this study clarify the potential errors in temperature measurement, i.e. induced by strain, and demonstrates the feasibility of the proof-of-concept mounting technique with "guide-tube" for cell level monitoring.

2. Materials and methods

2.1. Fabrication of the sensors

The FBGs used for this work were photo-inscribed using a Noria FBG Manufacturing System from NorthLab Photonics. This setup integrates a set of different phase masks, an ArF UV excimer laser (Coherent Excistar XS) emitting at 193 nm and all the optics required for FBG fabrication. The system provides a 1-D translational stage as well, allowing to accurately control the position of the optical fibre before the photo-inscription process. A hydrogen-loaded single-mode optical fibre (SMF-28) was placed on it to photo-inscribe 5 FBGs along the same fibre. The fiber coating was removed for FBG fabrication. Approximately 10 cm of the coating was removed so that all the FBGs were fabricated along this stripped portion of the fiber. This was convenient for fabrication, as well as to discard any additional strain effects that might arise from strain differences between the fiber and the coating materials, respectively, and due to the different thermal expansion coefficients of both materials. After the photo-inscription of each FBG, the fibre was shifted along its longitudinal axis and placed under the next phase-mask, repeating this sequence until the full FBG array was completed. The length of the FBGs was 5 mm each, and the pitch of the phase-masks were 1054 nm, 1063 nm, 1070 nm, 1075 nm and 1082 nm, respectively. The laser emission configuration was set to a pulse energy of 5 mJ and a repetition rate of 50 Hz, and each FBG was photo-inscribed by a single burst of 100 shots. The Refractive Index Modulation (RIM) induced on the fibres by using this manufacturing system occupies a broader region of the core [27], being the RIM more homogeneously distributed with regard to FBGs fabricated using other methods. Finally, the FBGs were kept at 100 °C for 36 h to remove the residual hydrogen content of the fibres and stabilise their thermal response while in operation.

2.2. Thermocouple sensors

This study uses two K-type thermocouples; these are a typical sensor used for battery surface temperature measurement [10,28,29]. A Reveltronics EGT-K 4 channel thermocouple amplifier produces a linear voltage relating to temperature experienced by the thermocouple sensors. Based on the AD8495 precision thermocouple amplifier with cold-junction compensation, the EGT-K amplifier converts thermocouple non-linear millivolts signal to 0–5 V

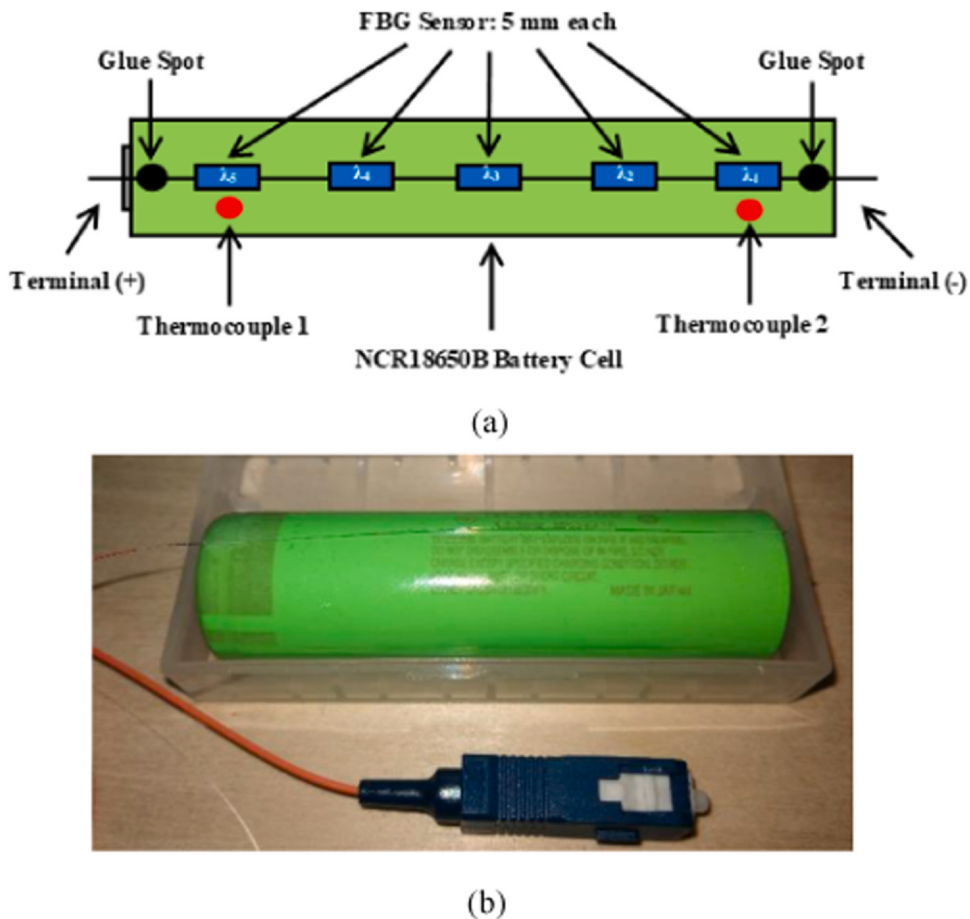


Fig. 1. Sensor configuration A: Illustration (a) and image of assembly (b) of the optical fibre with five FBG sensors placed along the length of the NCR18650B LIB.

linear analogue output. Where 0 V is 0 °C, and 5 V is equal to 1250 °C, the accuracy of this amplifier is $\pm 1.5\%$ with a conversion rate voltage of 4 mV/°C. The AD8495 thermocouple amplifier is explicitly designed for measurement using K-type thermocouples [18]. The temperature response of the thermocouples is calculated using $T = V_{out}/V_{CR}$, Where T is the temperature in degrees Celsius, V_{out} is the amplifier output voltage, and V_{CR} is the conversion rate voltage of the amplifier.

2.3. FBG sensor arrangement

Two sensor arrangements to evaluate the best practice for sensor adhesion on the battery are devised. In the first case, the optical fibre containing the sensors is glued at both ends of the battery (configuration A). In the second case, only one end of the fibre is glued to the battery, while the other end is attached to the battery via a "guide tube" which enables freedom of expansion (configuration B) of the fiber, i.e. as it is not directly attached to the battery via glue. Configuration A is depicted in Fig. 1, with the fibre containing the FBGs placed along the length of the cylindrical Panasonic NCR18650B LIB surface and a small amount of Micro-Measurements M-Bond 200 adhesive used at either end to attach the fibre to the surface. Configuration B, depicted in

Fig. 2, has the fibre placed along the length of the cylindrical surface and glued with the same aforementioned adhesive only at the negative terminal, i.e. thus attaching the fibre to the surface, while the other end of the battery utilises a PVC guide-tube, serving the purpose of keeping the fibre in the longitudinal direction. The use of the guide tube for the mounting of the FOS accommodates for the natural expansion and contraction of the battery cell without

affecting the FOSs, thus allowing the FBG sensors to capture only temperature variations from the cell surface. This contrasts with sensor configuration A where the FOS would experience strain due to the restrictive nature of the 2 fixed glue spots.

The Micro-Measurements M-Bond 200 adhesive used is a Cyanoacrylate type adhesive with an operational temperature range of -300 °C to +200 °C on the short-term and 25 °C to +150 °C on a long-term basis. In both configurations, the 5 FBGs were not directly attached to the battery surface; a slight slack remains in the length which allowed for some compensation from the natural expansion and contraction of the LIB due to internal pressure variation, while still allowing the FBGs close proximity to the LIB surface [25]. A k-type thermocouple at either end of the LIB surface is applied, directly opposite FBGs 1 and 5. Two thermocouples are used, i.e. instead of five, to avoid overcrowding on the battery surface, which might result in restricting or damaging the FOSs. These adhere to the surface with vinyl tape, which offers flexibility in the mounting position, i.e. the use of tape to adhere thermocouples to LIB surface is present in multiple studies [29–32].

2.4. Sensor calibration

Configuration A, with the optical fibre containing the sensors attached at both ends of the LIB, was calibrated over a temperature range of 10–40 °C ± 1 °C at increments of 10 °C, for at least 30 min. The FBG response over the 40 °C calibration schedule is shown in Fig. 3, which demonstrates agreement between the wavelength shift of the FBGs and the data from the thermocouples. The calibration and mean sensitivity of each FBG sensor over the chosen temperature range are shown in Fig. 3a, and

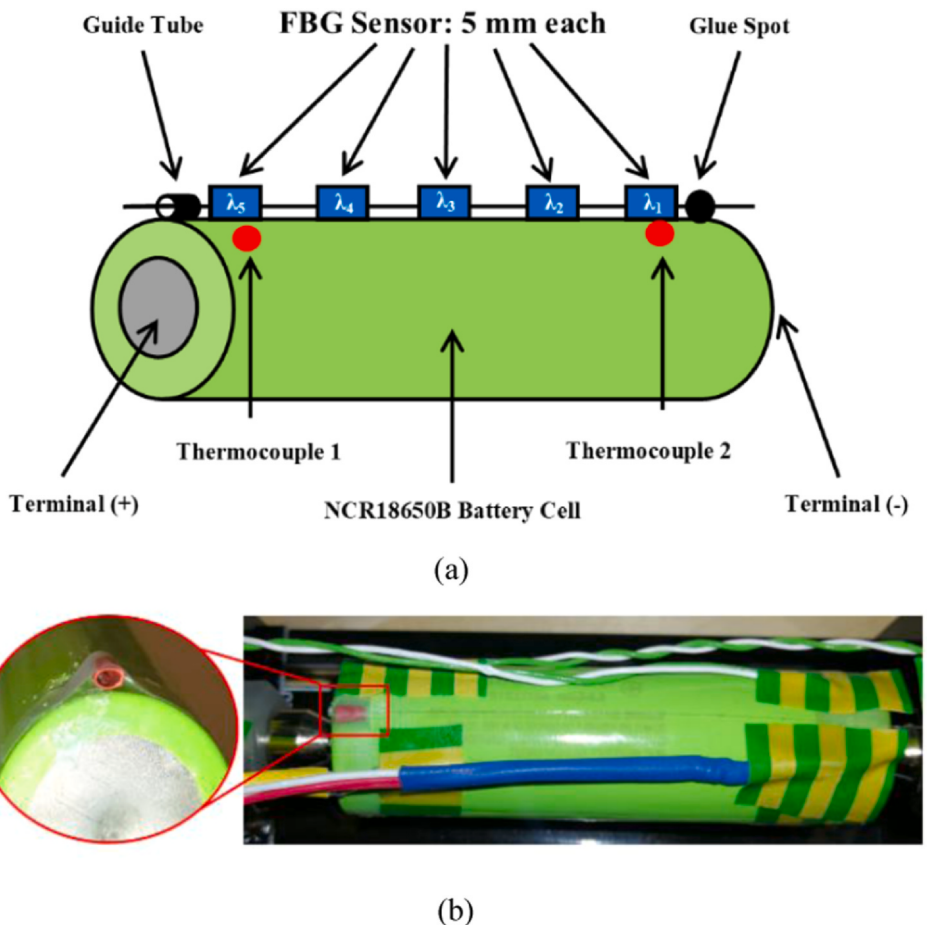


Fig. 2. Sensor configuration B: Illustration (a) and image of assembly (b) of the optical fibre with five FBG sensors placed along the length of the NCR18650B LIB, guide-tube represented with a close-up in (b).

Fig. 3b, respectively. The chamber maintained a fluctuation of $\pm 1^{\circ}\text{C}$ throughout the testing, which is visible for each temperature step in **Fig. 3a**. The fluctuation within the chamber is due to the maximum settings achievable with the current thermal chamber equipment. Taking the mean wavelength shift ($\Delta\lambda$) for each of the 5 FBG sensors over 30 min provides a single wavelength shift data-point. **Table 1** shows the shift in the mean wavelength for each FBG over this period.

Calculated for the four temperature exposure points, **Table 2** shows the standard deviation for all FBG measurements at the exposure temperatures. Thus, the method used herein accounts for fluctuation of temperature within the chamber; this method of calibration is similar to those presented in other studies with FBG sensors [9,10]. Using this method, the sensitivity of FBG sensors 1, 2, 3, 4 and 5 are 9.16, 8.90, 8.95, 8.99 and 9.12 pm/ $^{\circ}\text{C}$, respectively. It is important to note that the calibration is used to determine the sensitivity of each FBG at each exposure temperature, thus, does not account for LIB surface expansion, moreover the individual FBGs are in no instance attached to the battery surface over the stripped section of the FOS. For configuration B, the sensitivity factors are taken from the datasheet provided by the manufacturer for a 'free' fibre, i.e. where the optical fibre did not adhere to any surface. The sensitivity of FBGs 1, 2, 3, 4 and 5 are thus taken to be 9.80, 9.87, 9.93, 9.93 and 9.97 pm/ $^{\circ}\text{C}$, respectively. As the mounting of the fibre in configuration B is unrestricted in the sense that only one glue spot is utilised with the guide tube at one end, it is deemed appropriate that the manufacturers' sensitivity factor is sufficient for this mounting technique as the fibre has free movement in the longitudinal direction.

2.5. Data acquisition

The schematic of the data acquisition is detailed in **Fig. 4**, where the wavelength shifts corresponding to the 5 FBGs are acquired using a Micron Optics® sm125 FBG interrogator with the ENLIGHT® software. A PicoLog® 1012 data logger is used to record the output voltage of the Reveltronics thermocouple amplifier with the PicoLog® 6 software. A B&K Precision® 8601 DC programmable electronic load, is used to discharge the LIB, a B&K Precision® 9202 multi-range programmable DC power supply is used for charging. Data logging in the ENLIGHT®, PicoLog® 6 is set to 2 Hz while the B&K Precision® software is set at 1 Hz.

The thermal behaviour of the FBG sensors is defined by (1) [10,33], where k is the temperature sensitivity, λ_0 is the reference wavelength, and λ is the measured peak wavelength as a function of temperature.

$$\lambda = kT + \lambda_0 \quad (1)$$

Rearranging (1) provides the temperature:

$$T = \frac{(\lambda - \lambda_0)}{k} \quad (2)$$

The reference wavelength for both the configurations A and B are defined from the manufacturer as 1524.1 nm, 1537.1 nm, 1524 nm, 1554.2 nm and 1564.1 nm for FBG 1, 2, 3, 4 and 5 respectively. Thus, using (2) the thermal response of the LIB under the discharge conditions is derivable from the FBG signals.

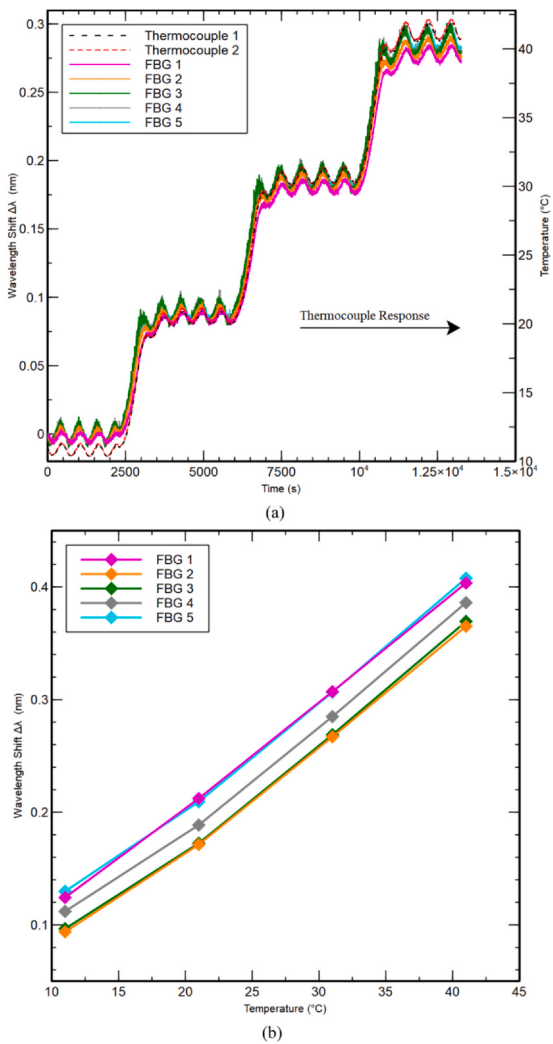


Fig. 3. FBG calibration sequence under configuration A: The wavelength shift over the calibration temperature variation (a), and (b); the resulting sensitivity over the 40 °C variation using 30 min averaged data.

2.6. LIB discharge technique

Ten-Watt constant power (CW) discharge induces a thermal reaction from the Panasonic NCR18650B LIB. This rate of discharge increases the LIB surface temperature by approximately 14 °C. An almost identical reaction from the LIB cell for both sensor configurations is shown in Fig. 5. During the discharge, as the voltage reduces at a varying rate, the current must increase in order to provide a CW output; thus, the current reacts with a significant upward inflection to counteract the downward Voltage inflection. A significant temperature change occurs in the LIB with the increased current, typically, the temperature increase follows the current increase [34], which makes the proposed setup an ideal technique for the purpose of temperature measurement. Both sensor configurations are subject

Table 2

Configuration A: wavelength shift standard deviation.

Temperature (°C)	FBG 1 (pm)	FBG 2 (pm)	FBG 3 (pm)	FBG 4 (pm)	FBG 5 (pm)
10	2.5	4.3	5.7	5.5	4.2
20	2.8	3.9	5.4	5.3	3.7
30	3.4	4.2	5.6	5.5	4.5
40	4.3	4.8	6.2	6.4	5.3

Wavelength shift standard deviation for each sensor in response to calibration temperature variation, pm = picometers.

to the same treatment, i.e. the LIB is charged at 1 C (3.4 A) Constant Current (CC) Constant Voltage (CV) at 4.2 Volts. During charging, the LIB is charged at 1 C until the voltage reaches maximum cell voltage, i.e. 4.2 V, upon which the charger switches to CV and the current gradually reduces until the cut-off current, i.e. 65 mA, is achieved. Before discharging, the cell must be in a state of rest for a minimum of 4 h to allow for internal balancing [35]. Two thermal chambers keep the LIB cells at the optimal temperature; one chamber is for storage purposes where cell resting occurs, and the other is for testing. Both chambers are at an optimal $25\text{ }^{\circ}\text{C} \pm 1\text{ }^{\circ}\text{C}$, which limits the temperature variance of the LIB cells between testing and resting phases.

3. Results and discussion

In order to determine the effectiveness of the mounting method's ability to isolate the temperature for reliable readings, the FBG response is compared directly to the thermocouple; however, it is crucial to discuss the temperature variation over the length of the LIB surface and the accuracy of the thermocouple system before comparing the FBG response with the thermocouples. The mean temperature difference between thermocouple 1 and 2, neglecting the error, is $0.2\text{ }^{\circ}\text{C}$ for sensor configuration A and $0.32\text{ }^{\circ}\text{C}$ for configuration B, both having a standard deviation of $0.09\text{ }^{\circ}\text{C}$. This shows that the thermocouples, i.e. placed at the opposite ends of the LIB surface, respond in a very similar way. Moreover, as the thermocouples experience only a small temperature variation over the length of the surface during the stated discharge process, it is reasonable to assume the resulting FBG temperature readings do not become distorted by a varying temperature differential over the cell surface for both sensor configurations.

As discussed previously, the accuracy of the thermocouple amplifiers is $\pm 1.5\%$. Considering this for both the sensor configurations during the LIB discharge; for Sensor configuration A, thermocouple 1 and 2 demonstrates a minimum and maximum error of $0.36\text{ }^{\circ}\text{C}$ and $0.58\text{ }^{\circ}\text{C}$ respectively, with a standard deviation of $0.04\text{ }^{\circ}\text{C}$. In terms of Sensor configuration B, thermocouple 1 ranges from a minimum error of $0.37\text{ }^{\circ}\text{C}$ to a maximum error of $0.58\text{ }^{\circ}\text{C}$, with a standard deviation of $0.04\text{ }^{\circ}\text{C}$. Comparatively, thermocouple 2 experiences a minimum and maximum error of $0.38\text{ }^{\circ}\text{C}$ and $0.59\text{ }^{\circ}\text{C}$ respectively, with a standard deviation of $0.04\text{ }^{\circ}\text{C}$. Fig. 6 shows the response of the thermocouples and the corresponding temperature error throughout the LIB discharge for both sensor configurations. As can be seen from Fig. 6, both thermocouples, incorporating allowable error from the thermocouple amplifier, behave in an almost identical manner. This

Table 1

Configuration A: Mean FBG wavelength of calibration.

Temperature (°C)	FBG 1 (nm)	FBG 2 (nm)	FBG 3 (nm)	FBG 4 (nm)	FBG 5 (nm)
10	1524.22	1537.18	1547.08	1554.30	1564.22
20	1524.31	1537.27	1547.17	1554.39	1564.31
30	1524.41	1537.37	1547.27	1554.48	1564.41
40	1524.50	1537.47	1547.37	1554.59	1564.51

Mean wavelength of each FBG at each calibration temperature variation, 30 min averaged data, nm = nanometres.

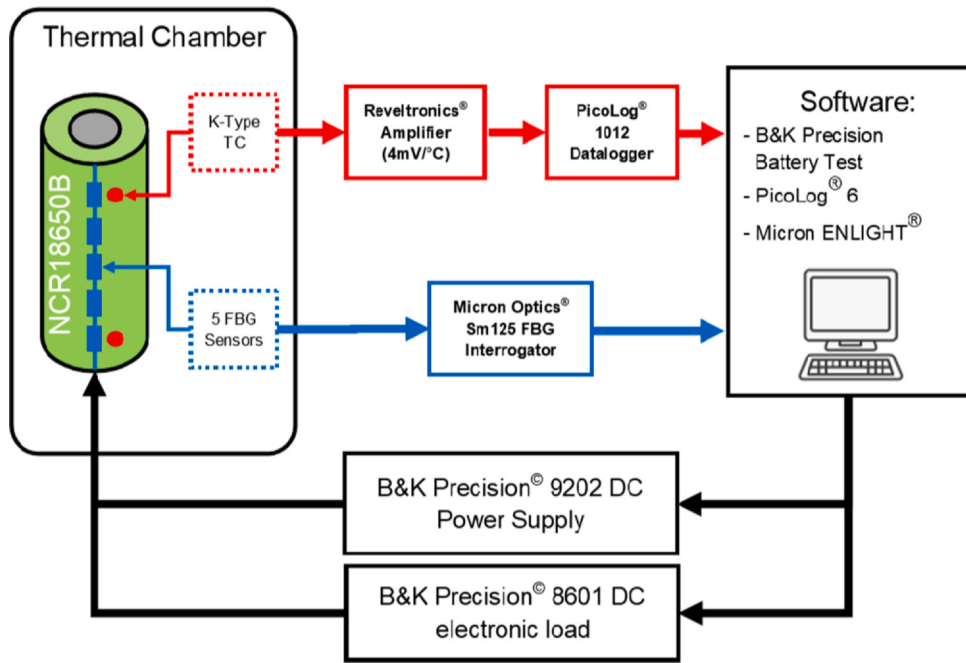


Fig. 4. Detailed diagram of the data acquisition setup.

further suggests a uniform temperature variation over the LIB surface during discharge. Comparing both sensor configurations, it is evident that the mounting techniques play a vital role in the resulting temperature sensing. The resulting variation in temperature (ΔT) for both sensor arrangements is shown in Fig. 7, and as can be seen, for sensor configuration A, the temperature measurement of each of the FBG signals is not consistent, and indeed, in the most extreme case, a difference of 8.5°C between FBG3, FBG4 and FBG1, could be observed. On the other hand, sensor configuration B (Fig. 7b) demonstrates a more consistent and uniform measurement of temperature along the LIB surface with a maximum temperature difference of 2.13°C . In correlation to thermocouples, thus, the use of the guide-tube shows a significant improvement on the ability of the FBG sensors to measure the temperature of the LIB. The variation in temperature (ΔT) of the FBG sensors and thermocouples against the

discharge current (ΔI) over the discharge period, is illustrated in Fig. 8.

The purpose of the discharge tests is to evaluate the performance of the FOSs, i.e. under the two configurations, with respect to discharge current. The change in current (ΔI) of each discharge experiment is consistent, and therefore, it is reasonable to assume similar temperature differentials within the LIB. The analysis demonstrates the increase in temperature differential with increasing load current on the LIB. It is clear from the obtained measurements that enabling free movement with the addition of the 'guide-tube' results in significantly more accurate measurements. The results in both Fig. 7 and Fig. 8, demonstrate that sensor configuration B, i.e. with the guide-tube, is more suitable to measure the temperature of the cylindrical LIB surface. When compared to the thermocouples, sensor configuration A generally displays an accuracy of $\pm 4.25^{\circ}\text{C}$

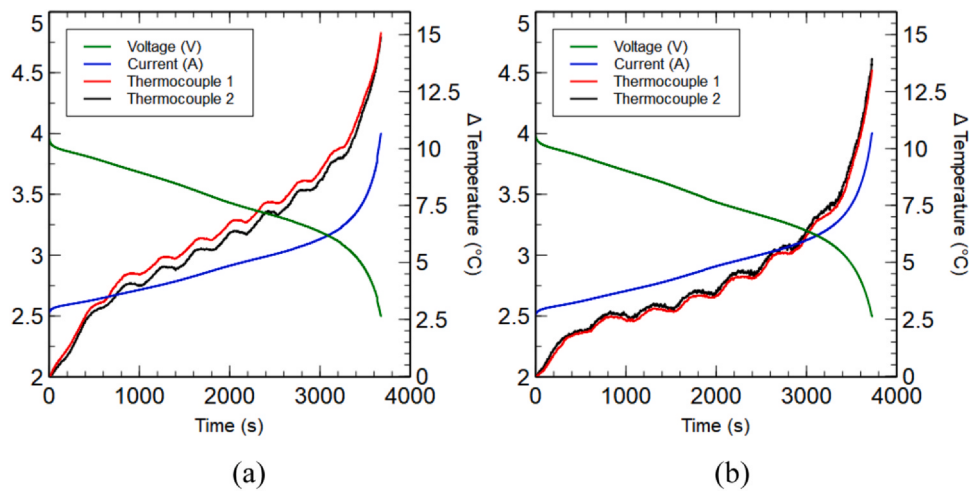


Fig. 5. 10-Watts CW discharge: Voltage and current inflections and comparable thermal variance by thermocouples for sensor configuration A (a); and Sensor configuration B (b).

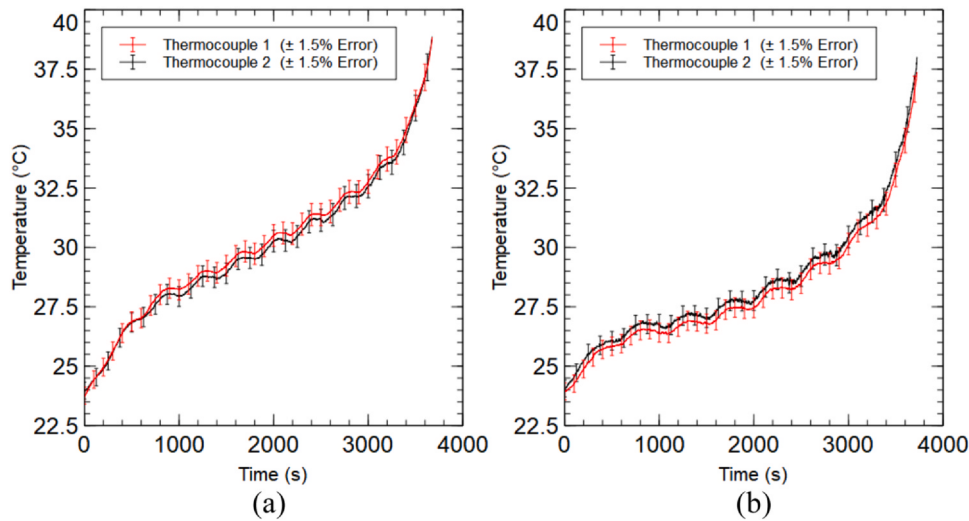


Fig. 6. Temperature response of thermocouples during LIB Discharge (a) configuration A (b), configuration B, demonstrating amplifier error of $\pm 1.5\%$.

(8.5 $^{\circ}\text{C}$ variance), which is reduced to +2.13 $^{\circ}\text{C}$ (2.13 $^{\circ}\text{C}$ variance) in configuration B with the strain-relief of the guide-tube in place.

These results demonstrate that the behaviour of each FBG is not consistent between the two sensor configurations; both Fig. 7 and Fig. 8 illustrate that configuration A has the highest variation in temperature for FBG1, however, under sensor configuration B, this is not the case, as FBG1 and FBG2 indicate an almost identical response. In both configurations FBG5 exhibit a similar response, whereas FBGs 3 and 4 exhibit the most considerable difference in measurement, compared to the responses from the thermocouples.

It is reasonable to conclude that sensor configuration A, i.e. with two glue spots on either end of the sensing region, induces sufficient strain on the FBGs and hence influences the temperature measurements significantly; to the point inaccuracies render the data ineffective analytically. Sensor configuration B, i.e. mounting technique with guide-tube, demonstrates promising results, where the response from the FBGs are closely related to that of thermocouple sensors, this is due to the guide-tube allowing the optical fibre containing the FBGs to act independently of strain induced by internal pressure fluctuations within the LIB. It is essential to

highlight that although sensor configuration B provides a more accurate representation of the LIB, the recorded temperatures do not come within the error margin of the thermocouples, except for FBG5, which demonstrates a response across both thermocouples, including allowable error. However, the aim of this work was to evaluate the suitability of the guide-tube technique to attach the FOSs on the battery surface. The results demonstrate that this is possible and the sensors measurements are comparable to that of thermocouples, which were directly attached to the LIB. The results demonstrate that submergence of the sensing region with a binding agent is not necessary. This enables multiple benefits including the reduction of the amount of chemicals needed, the risk of chemical reaction with the battery and increases ease of handling, i.e. each thermocouple requires separate wiring while all the 5 FOSs were along a single fibre strand of less than 1 cm diameter. However, fine-tuning of the FBG sensors are required in order to make measurements that are within the acceptable error margin. For example, physical parameters of the FBG can be optimised, i.e. the length of the FBG could be longer. Work is ongoing to investigate this further.

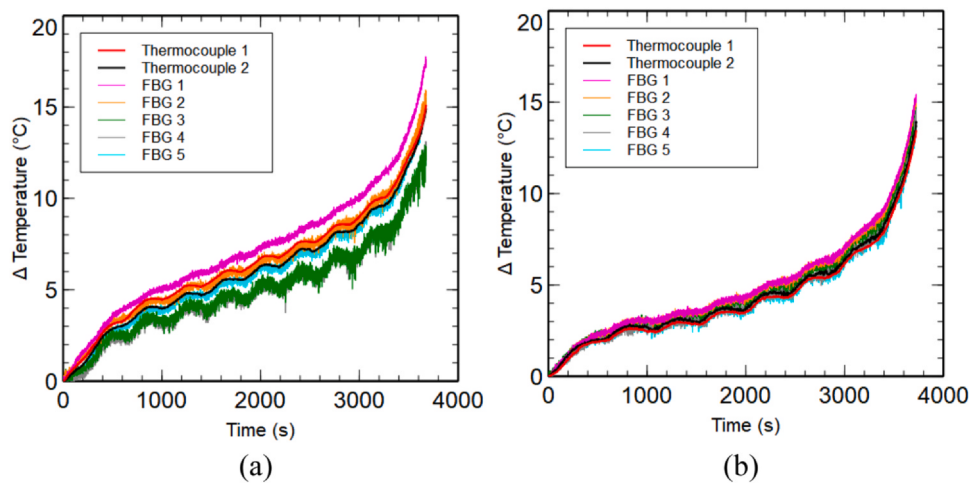


Fig. 7. Temperature response of FBGs under Sensor configuration A (a) and configuration B (b), compared to the measurements obtained by the thermocouples.

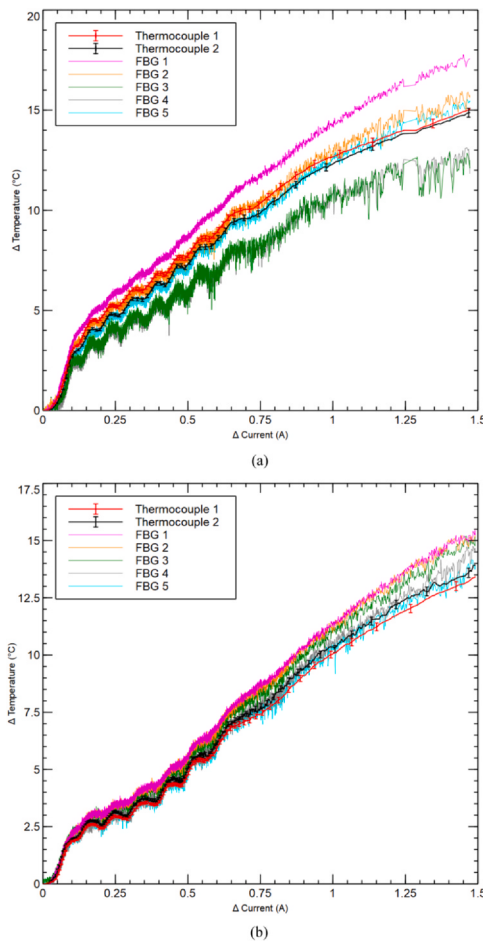


Fig. 8. FBG Temperature variation related to discharge current variation: Sensor configuration A (a), and Sensor configuration B (b), compared to the measurements obtained by the thermocouples.

4. Conclusion

The motivation for this research was to conduct a proof of concept on the guide-tube technique for the measurement of temperature of LIBs without having to attach the entire length of the fibre with a binding agent. In fact, a multitude of literature provides work on such FBG sensors which are submerged in a binding agent, i.e. to attach the sensors to the LIB, but are then susceptible to strain. The target for the proof of concept, therefore, was to evaluate the possibility of attaching the FBGs on the LIB in a manner that enables (a) the measurement of temperature without the use of a binding agent on the sensing region, and thus (b) having no susceptibility to strain. The results demonstrate that this is possible with the guide-tube technique that is proposed.

Furthermore, the work presented herein demonstrates the importance of the application of appropriate mounting techniques for optical fibre when used for the measurement of LIB temperature. The strain-induced on FBGs is sufficient to render the temperature measurements inaccurate, without careful placement of the fibre. The proposed guide-tube method provides a suitable solution for mounting an optical fibre strand, with multiple FBGs incorporated along its length, on a LIB, to reduce strain effects and thus more accurately record the temperature and hence improve the overall performance of LIB thermal monitoring. The accuracy of the temperature readings, when compared to thermocouples, is improved from $\pm 4.25^\circ\text{C}$ (8.5°C variation) to $\pm 2.13^\circ\text{C}$ (2.13°C variation) when the guide-tube mounting method is adopted. Work is ongoing to

refine the technique further to enable its suitability and practicality to be utilised in the EV industry.

CRediT authorship contribution statement

Keith M. Alcock: Investigation, Conceptualization, Methodology, Writing – original draft, Writing – reviewing & editing, Visualization. **Markus Grammel:** Investigation, Data curation, Visualization. **Álvaro González-Vila:** Conceptualization, Resources. **Leonardo Binetti:** Software, Resources. **Keng Goh:** Supervision, Conceptualization. **Lourdes S. M. Alwis:** Supervision, Conceptualization, Writing – reviewing & editing.

Declaration of Competing Interest

The authors declare that they have no known competing financial interests or personal relationships that could have appeared to influence the work reported in this paper.

References

- [1] S. Srdic, S. Lukic, Toward extreme fast charging: challenges and opportunities in directly connecting to medium-voltage line, IEEE Electrification Mag. 7 (2019) 22–31, <https://doi.org/10.1109/mele.2018.2889547>
- [2] A. Hnatov, S. Arhun, K. Tarasov, H. Hnatova, V. Mygal, A. Patlins,in: Proceedings of the IEEE 60th International Scientific Conference on Power and Electrical Engineering of Riga Technical University (RTUCON), (2019) 1–6. doi:10.1109/RTUCON48112.2019.8982352.
- [3] X.G. Yang, S. Ge, N. Wu, Y. Mao, F. Sun, C.Y. Wang, All-climate battery technology for electric vehicles: inching closer to the mainstream adoption of automated driving, IEEE Electrification Mag. 7 (2019) 12–21, <https://doi.org/10.1109/MELE.2018.2889545>
- [4] M. Tariq, A.I. Maswood, C.J. Gajanayake, A.K. Gupta, 2016 Ieee Symp. . Comput. Appl. Ind. Electron Iscaie (2016) 149–154, <https://doi.org/10.1109/iscaie.2016.7575054>
- [5] X. Feng, M. Ouyang, X. Liu, L. Lu, Y. Xia, X. He, Thermal runaway mechanism of lithium ion battery for electric vehicles: A review, Energy Storage Materials 10 (2018) 246–267, <https://doi.org/10.1016/j.ensm.2017.05.013>
- [6] J. Meyer, A. Nedjalkov, A. Doering, M. Angelmahr, W. Schade, SPIE Proceedings, Fiber Optic Sensors and Applications XII 9480 (2015), <https://doi.org/10.1117/12.2183325>
- [7] S.S. Zhang, K. Xu, T.R. Jow, Charge and discharge characteristics of a commercial LiCoO₂-based 18650 Li-ion battery, Journal of Power Sources 160 (2006) 1403–1409, <https://doi.org/10.1016/j.jpowsour.2006.03.037>
- [8] J. Meyer, A. Nedjalkov, E. Pichler, C. Kelb, W. Schade, Development of a Polymeric Arrayed Waveguide Grating Interrogator for Fast and Precise Lithium-Ion Battery Status Monitoring, batteries 5 (4) (2019) 66, <https://doi.org/10.3390/batteries5040066>
- [9] G. Yang, C. Leitão, Y. Li, J. Pinto, X. Jiang, Real-time temperature measurement with fiber Bragg sensors in lithium batteries for safety usage, Measurement 46 (9) (2013) 3166–3172, <https://doi.org/10.1016/j.measurement.2013.05.027>
- [10] M. Nascimento, M.S. Ferreira, J.L. Pinto, Real time thermal monitoring of lithium batteries with fiber sensors and thermocouples: a comparative study, Measurement 111 (2017) 260–263, <https://doi.org/10.1016/j.measurement.2017.07.049>
- [11] A. Fortier, M. Tsao, N.D. Williard, Y. Xing, M.G. Pecht, Preliminary study on integration of fiber optic bragg grating sensors in li-ion batteries and in situ strain and temperature monitoring of battery cells, Energies 10 (7) (2017), <https://doi.org/10.3390/en10070838>
- [12] E. Gümuşsu, Ö. Ekici, M. Köksal, 3-D CFD modeling and experimental testing of thermal behavior of a Li-Ion battery, Appl. Therm. Eng. 120 (2017) 484–495, <https://doi.org/10.1016/j.applthermaleng.2017.04.017>
- [13] C. Essl, A.W. Golubkov, E. Gasser, M. Nachtnebel, A. Zankel, E. Ewert, A. Fuchs, Comprehensive hazard analysis of failing automotive lithium-ion batteries in overtemperature experiments, Batteries 6 (2) (2020), <https://doi.org/10.3390/batteries6020030>
- [14] L.W. Traub, Calculation of constant power lithium battery discharge curves, Batteries 2 (2) (2016), <https://doi.org/10.3390/batteries2020017>
- [15] Y. Zhao, Q. Li, B. Zou, T. Zhang, L. Jin, G. Qiao, B. Nie, Y. Huang, Y. Ding, Performance of a liquid cooling-based battery thermal management system with a composite phase change material, Int. J. Energy Res. 44 (2020) 4727–4742, <https://doi.org/10.1002/er.5254>
- [16] C.R. Birk, M.R. Roberts, E. McTurk, P.G. Bruce, D.A. Howey, Degradation diagnostics for lithium ion cells, J. Power Sources 341 (2017) 373–386, <https://doi.org/10.1016/j.jpowsour.2016.12.011>
- [17] J. Fleming, T. Amietszajew, E. McTurk, D. Greenwood, R. Bhagat, Development and evaluation of in-situ instrumentation for cylindrical Li-ion cells using fibre optic sensors, HardwareX 3 (2018) 100–109, <https://doi.org/10.1016/j.hrx.2018.04.001>

- [18] M. Duff, J. Towey, Two Ways to Measure Temperature Using Thermocouples Feature Simplicity, Accuracy, and Flexibility, *Analog Dialogue* 44 (4) (2010) 3–8.
- [19] H. Chikh-Bled, K. Cah, A. Gonzalez-Vila, B. Lasri, C. Caucheteur, Behavior of femtosecond laser-induced eccentric fiber Bragg gratings at very high temperatures, *Opt. Lett.* 41 (17) (2016) 4048–4051, <https://doi.org/10.1364/OL.41.004048>
- [20] W.R. Habel, Optical Fiber Methods in Nondestructive Evaluation, in *Handbook of Advanced Nondestructive Evaluation* (2019) 595–642, doi: 10.1007/978-3-319-26553-7_39.
- [21] A. Raghavan, P. Kiesel, L.W. Sommer, J. Schwartz, A. Lochbaum, A. Hegyi, A. Schuh, K. Arakaki, B. Saha, A. Ganguli, K.H. Kim, C.A. Kim, H.J. Hah, S.K. Kim, G.O. Hwang, G.C. Chung, B. Choi, M. Alamgir, Embedded fiber-optic sensing for accurate internal monitoring of cell state in advanced battery management systems part 1: cell embedding method and performance, *J. Power Sources* 341 (2017) 466–473, <https://doi.org/10.1016/j.jpowsour.2016.11.104>
- [22] S. Novais, M. Nascimento, L. Grande, M.F. Domingues, P. Antunes, N. Alberto, C. Leitão, R. Oliveira, S. Koch, G.T. Kim, S. Passerini, J. Pinto, Internal and external temperature monitoring of a li-ion battery with fiber bragg grating sensors, *Sensors* 16 (2016) 1394, <https://doi.org/10.3390/s16091394> PMID - 27589749
- [23] Micael Nascimento, Susana Novais, Catia Leitão, M. Fátima Domingues, Nélia Alberto, Paulo Antunes, and João L. Pinto "Lithium batteries temperature and strain fiber monitoring", Proc. SPIE 9634, 24th International Conference on Optical Fibre Sensors, 96347V (28 September 2015), doi:10.1117/12.2195218.
- [24] E. McTurk, T. Amietszajew, J. Fleming, R. Bhagat, Thermo-electrochemical instrumentation of cylindrical Li-ion cells, *J. Power Sources* 379 (2018) 309–316, <https://doi.org/10.1016/j.jpowsour.2018.01.060>
- [25] L.W. Sommer, A. Raghavan, P. Kiesel, B. Saha, T. Staudt, A. Lochbaum, A. Ganguli, C.J. Bae, M. Alamgir, Embedded fiber optic sensing for accurate state estimation in advanced battery management systems, *Mrs Proc.* 1681 (2014), <https://doi.org/10.1057/opl.2014.560> mrss14-1681-q01-03.
- [26] A. Ramanujam, P. Sankaranarayanan, A. Vasan, R. Jayaprakash, V. Sarangan, A. Sivasubramaniam, e-Energy '17: in proceedings of the The Eighth International Conference on Future Energy Systems, (2017) 228–233, doi: 10.1145/3077839.3077854.
- [27] Á. González-Vila, A. Ioannou, M. Loyez, M. Deblliquy, D. Lahem, C. Caucheteur, Surface plasmon resonance sensing in gaseous media with optical fiber gratings, *Opt. Lett.* 43 (2018) 2308–2311, <https://doi.org/10.1364/OL43.002308>
- [28] Y. Xie, J. Zheng, W. Li, K. Lee, Y. Zhang, J. Liu, D. Dan, C. Wu, P. Wang, An improved electrothermal-coupled model for the temperature estimation of an air-cooled battery pack, *Int. J. Energy Res.* 44 (2019) 2037–2060, <https://doi.org/10.1002/er.5058>
- [29] T.H. Dubaniewicz Jr., J.P. DuCarme, Are lithium ion cells intrinsically safe? *IEEE Trans. Ind. Appl.* 49 (6) (2013) 2451–2460, <https://doi.org/10.1109/TIA.2013.2263274>
- [30] S. Panchal, M. Mathew, R. Fraser, M. Fowler, Electrochemical thermal modeling and experimental measurements of 18650 cylindrical lithium-ion battery during discharge cycle for an EV, *Appl. Therm. Eng.* 135 (2018) 123–132, <https://doi.org/10.1016/j.applthermaleng.2018.02.046>
- [31] S. Panchal, I. Dincer, M. Agelin-Chaab, R. Fraser, M. Fowler, Experimental temperature distributions in a prismatic lithium-ion battery at varying conditions, *Int. Commun. Heat. Mass Transf.* 71 (2016) 35–43, <https://doi.org/10.1016/j.icheatmasstransfer.2015.12.004>
- [32] K.K. Parsons, T.J. Mackin, Design and simulation of passive thermal management system for lithium-ion battery packs on an unmanned ground vehicle, *J. Therm. Sci. Eng. Appl.* 9 (1) (2017), <https://doi.org/10.1115/1.4034904>
- [33] Rd.S. Marques, A.R. Prado, P.Fd.C. Antunes, P.Sd.B. André, M.R.N. Ribeiro, A. Frizera-Neto, M.J. Pontes, Corrosion resistant FBG-based quasi-distributed sensor for crude oil tank dynamic temperature profile monitoring, *Sensors* 15 (12) (2015) 30693–30703, <https://doi.org/10.3390/s151229811>
- [34] A. Mills, S. Al-Hallaj, Simulation of passive thermal management system for lithium-ion battery packs, *J. Power Sources* 141 (2) (2005) 307–315, <https://doi.org/10.1016/j.jpowsour.2004.09.025>
- [35] A. Barai, G.H. Chouchelamane, Y. Guo, A. McGordon, P. Jennings, A study on the impact of lithium-ion cell relaxation on electrochemical impedance spectroscopy, *J. Power Sources* 280 (2015) 74–80, <https://doi.org/10.1016/j.jpowsour.2015.01.097>



Keith M. Alcock received the BEng (Hons) degree in Energy & Environmental Engineering in 2015 and the master degree in Renewable Energy in 2016, both from Edinburgh Napier University, UK. At the same establishment, he is currently pursuing the PhD degree in Engineering, focusing on lithium-ion battery thermal management utilising foam and phase change materials



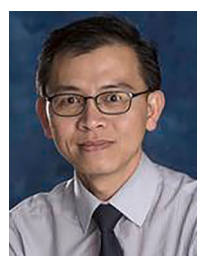
Markus Grammel participated in a double bachelor's degree program in 2020 and graduated in Engineering with Management (B.Eng. Hons) from Edinburgh Napier University and Business Administration and Engineering (B.Sc.) from Hochschule Furtwangen University (Germany). Currently, he is pursuing a master's degree in Technical Management at Hochschule Heilbronn in Germany.



Álvaro González-Vila received his Master degree in Telecommunications Engineering in 2014 from the University of Cantabria, Spain. He then obtained his Ph.D. degree in Engineering Science and Technology in 2019 from the University of Mons, Belgium, being his research focused on advanced coatings for optical fibre sensors. He was the holder of a FRIA grant from the Belgian F.R.S.-FNRS and is a member of the OSA and SPIE. He currently works at IKERLAN Technology Research Centre (Basque Research and Technology Alliance, BRTA) as a R&D Engineer on IoT and embedded systems



Leonardo Binetti, completed his Bachelor degree in Materials Science at the University of Bari, Italy in 2015. He then successfully obtained a Masters (with Distinction) in Advanced Materials Engineering at Edinburgh Napier University, UK in 2018. He is currently pursuing a PhD in Photonics and Surface Chemistry at Edinburgh Napier University, UK.



Keng Goh graduated with BEng (Hons) degree in Electrical & Electronic and PhD in Nonlinear Control system application from University of Leicester in 1998 and 2004 respectively. In between these studies, he worked with Hewlett Packard for two years as instrumentation engineer. He is currently Lecturer at Edinburgh Napier University



Lourdes S. M. Alwis completed her PhD thesis in the field of grating-based Fiber Optic Sensors in 2013 at City, University of London, UK, while working for R&D of Alcatel-Lucent Ltd. She currently works at Edinburgh Napier University as a Lecturer. Her research interests include wearable technology and photonic sensors that can be used for Civil, Biomedical and Chemical engineering applications.